

1D TIME-DOMAIN SOLUTION FOR SEISMIC GROUND MOTION PREDICTION

By Jian-Ye Ching¹ and Steven D. Glaser²

ABSTRACT: A full time-domain solution for predicting earthquake ground motion based on the 1D viscoelastic shear-wave equation is presented. The derivation results in a time-domain equation in the form of an infinite impulse response filter. A solution in the time domain has several advantages including causality, direct modeling of impulsive and transient processes, and ease of inclusion of nonlinear soil behavior. The method is applicable to any arbitrarily layered silhouette presented as SH-wave velocity, damping coefficient, and mass density profiles for designated soil intervals. For nonlinear evaluations, an equivalent-linear formulation is incorporated and the standard modulus and damping degradation curves become part of the input set. Input motion can be either rock-outcrop or body-wave motions measured or estimated at the bottom of the geologic profile, and the output is the estimated ground motion time history. Application of the method to vertical array strong motion records from Garner Valley, and Wildlife Site, Calif., shows that predicted surface (and interval) ground motion is virtually identical to that measured. The differences between the results of linear and nonlinear analyses are negligible for most cases. A comparison of the time-domain model with SHAKE shows that SHAKE fails to accurately predict time histories in some situations, whereas the time-domain solution always yields satisfactory predicted surface ground motions.

INTRODUCTION

The purpose of this work is to show that the linear solution of the 1D viscoelastic wave equation can predict seismic ground motions accurately without any model calibration (as long as the soil remains a solid). Furthermore, the exact solution of the 1D viscoelastic wave equation can be written, given mild assumptions, as a time-domain infinite impulse response (IIR) filter with its attendant computational advantages [e.g., Kanasevich (1981) and Oppenheim and Schaffer (1989)].

The time-domain solution has three attractive attributes: (a) computational problems such as frequency-domain aliasing can be avoided; (b) time-domain methods are capable of directly incorporating nonlinear and time-varying behaviors; and (c) the time-domain approach preserves causality (i.e., “history”) and maintains the arrow of time. Traditionally, evaluation of the wave equation solution has been made in the frequency domain because the desired calculations are much faster. The frequency-domain solutions assume that the process (event) being modeled is best represented by a set of orthogonal basis functions of harmonic sinusoids without beginning or end. Earthquake ground motion, however, is causal, transient, and far from harmonic, so the time-domain solution is intuitively more suitable for estimating earthquake ground motions.

The model is validated here using case histories from Garner Valley, and Wildlife Site, Calif., seismic vertical arrays. With the vertical array data, the motions predicted by the model for various positions in the ground can be directly compared to the actual ground motions. Linear and nonlinear (based on the equivalent-linear approach) analyses are conducted. Equivalent blind predictions of time-domain results from SHAKE (Schnabel et al. 1972) are also studied in this paper for the purpose of comparison.

Previous Methods for Seismic Ground Motion Estimation

Accurate prediction of seismic site response has been one of the main goals of the earthquake engineering community. Several early developments in the 1970s, including SHAKE (Schnabel et al. 1972), DESRA-2 (Finn et al. 1976), and CHARSOIL (Streeter et al. 1973), were major steps toward this goal. SHAKE is a frequency-domain analysis of a 1D shear-wave equation with hysteretic damping. The nonlinearity of soils is incorporated into the model by the equivalent-linear approach.

DESRA-2 solves the 1D nonlinear shear-wave equation in the time domain and incorporates viscous/hysteretic damping. The approach assumes a lumped mass soil system and applies the wave equation into a system of lumped mass equations. The soil nonlinearity is taken into account by assuming soils behave according to the hyperbolic model for initial loading and the Masing criterion for unloading/reloading. DESRA-2 was generalized to a 2D time-domain nonlinear analysis, TARA-3 (Finn et al. 1986). CHARSOIL solves a set of equations similar to DESRA-2, using a characterization equation method while assuming soil moduli and damping ratios vary with shear strain according to the Ramberg-Osgood model for initial loading and Masing criterion for unloading/reloading.

More recently, efforts have been made to develop more sophisticated constitutive laws of soils (Prevost 1978; Pyke 1979; Iai et al. 1992; Pestana and Whittle 1999; Borja et al. 2000). Availability of faster computers enables incorporation of these newly developed constitutive laws with 2D or 3D numerical analyses (e.g., finite-element and finite-difference methods).

Concurrent with these developments, relevant aspects of the 1D (and 2D) wave propagation problem have been extensively examined by seismologists, albeit usually to solve a problem different than the one here—imaging the earth’s interior using reflection seismology. One example is the theoretical method introduced by Goupillaud (1961) and developed by Claerbout (1968), Robinson and Silvia (1979), and Silvia and Robinson (1979). The Goupillaud approach solves for 1D wave propagation directly in the time domain, with the “limiting” assumption that signal travel time in each arbitrary layer is identical. Frankel and Vidale (1992) solved a full 3D seismic wave propagation problem using a finite-difference method accurate to the fourth order in space and second order in time. Most recently, Zeng and Anderson (1995) proposed a semi-3D so-

¹Grad. Student Res., Dept. of Civ. and Envir. Engrg., Univ. of California, Berkeley, CA 94720.

²Assoc. Prof., Dept. of Civ. and Envir. Engrg., Univ. of California, Berkeley, CA.

Note. Discussion open until June 1, 2001. To extend the closing date one month, a written request must be filed with the ASCE Manager of Journals. The manuscript for this paper was submitted for review and possible publication on February 17, 1999. This paper is part of the *Journal of Geotechnical and Geoenvironmental Engineering*, Vol. 127, No. 1, January, 2001. ©ASCE, ISSN 1090-0241/01/0001-0036-0047/\$8.00 + \$.50 per page. Paper No. 20286.

lution for seismic wave propagation in layered media based on the generalized reflection and transmission matrix method (Luco and Apsel 1983).

THEORY OF 1D SHEAR-WAVE PROPAGATION IN LAYERED MEDIA

Frequency-Domain Analytical Solution

Solve the equation of 1D viscoelastic shear-wave propagation through layered media

$$\rho \cdot \partial^2 u / \partial t^2 = G \cdot \partial^2 u / \partial x^2 + \eta \cdot \partial^3 u / \partial x^2 \partial t \quad (1)$$

where u = shear displacement; ρ = mass density; G = shear modulus; and η = viscous damping coefficient. By accepting (1), one assumes that (a) earthquake ground motions consist only of vertically propagating shear waves; (b) soils are idealized as horizontal layers; and (c) soil is homogenous within each layer. Fig. 1 shows one example of the idealized soil model. The analytical solution is found by applying appropriate boundary conditions. The resulting displacement can be written (Schnabel et al. 1972)

$$u(x_j, \omega) = E_j(\omega) \cdot e^{ik_j x_j} + F_j(\omega) \cdot e^{-ik_j x_j} \quad (2a)$$

where

$$E_j(\omega) = 0.5 \cdot E_{j-1}(1 + \alpha_{j-1}) \cdot e^{ik_{j-1} h_{j-1}} + 0.5 \cdot F_{j-1}(1 - \alpha_{j-1}) \cdot e^{-ik_{j-1} h_{j-1}} \quad (2b)$$

$$F_j(\omega) = 0.5 \cdot E_{j-1}(1 - \alpha_{j-1}) \cdot e^{ik_{j-1} h_{j-1}} + 0.5 \cdot F_{j-1}(1 + \alpha_{j-1}) \cdot e^{-ik_{j-1} h_{j-1}} \quad (2c)$$

$$E_{\text{rock}}(\omega) = 0.5 \cdot E_m(1 + \alpha_m) \cdot e^{ik_m h_m} + 0.5 \cdot F_m(1 - \alpha_m) \cdot e^{-ik_m h_m} \quad (2d)$$

$$U_j(\omega) = E_j(\omega) + F_j(\omega) \quad (2e)$$

$$E_1(\omega) = F_1(\omega) \quad (2f)$$

$$\alpha_j(\omega) = \sqrt{[\rho_j(G_j + i\omega\eta_j)] / [\rho_{j+1}(G_{j+1} + i\omega\eta_{j+1})]} \quad (2g)$$

$$k_j(\omega) = \omega \sqrt{\rho_j / (G_j + i\omega\eta_j)} \quad (2h)$$

where E_j is interpreted as the upgoing wave; F_j = downgoing wave at the j th interface; E_{rock} = upgoing wave at the soil-rock interface; k_j , h_j , G_j , and η_j = complex wave number, thickness,

shear modulus, and viscous damping coefficient, respectively, of the j th layer; α_j = impedance ratio at the $(j + 1)$ th interface; x_j = local coordinate of the j th layer; and U_j = resulting displacement at the j th interface.

Schnabel et al. (1972) stated that the damping ratio β is related to η by the following equation:

$$G + i\omega\eta = G \cdot (1 + 2i\beta) \quad \text{or} \quad \beta = (\omega \cdot \eta) / 2G \quad (3)$$

where ω = angular frequency. This equation originates from the belief that G and β of many soils are nearly independent of frequency (Schnabel et al. 1972). In mechanical vibration theory, this frequency-independent model is called the ideal hysteretic or structural damping model (Crandall 1991). The discussion section will show that (3) introduces serious contradictions into the solution.

Discrete Time-Domain Solution Composed of Transient Functions

The derivation of the time-domain solution is based on the analytical frequency-domain solutions [(2)], with incorporation of the viscous damping model

$$\tau = G \cdot \gamma + \eta \cdot \dot{\gamma} \quad (4)$$

where τ and γ = shear stress and strain, respectively. This model assumes the specific damping is proportional to the loading frequency and can be formulated easily in the time domain (the hysteretic damping model cannot be formulated easily in the time domain because it is noncausal, as discussed later). The viscous damping model does not capture the frequency-independent behavior of soil and, similar to the hysteretic damping assumption, is used as an approximation.

For the frequency-domain solutions, the basis functions are regarded as linear combinations of infinite in time steady-state sinusoids at arbitrary amplitudes, frequencies, and phase shifts. Mathematically representing transients by steady-state harmonics is possible, because any stable piecewise-continuous function can be represented by an infinite summation of steady-state sinusoid functions. For earthquakes, however, one only has discrete time-domain approximations of transient ground motions, rather than analytical frequency-domain steady-state signals. One purpose of this work is to reformulate (2) as a discrete time-domain solution composed of transient functions.

The derivation begins by taking the Z transform (Oppenheim and Schaffer 1989), the discrete "equivalent" of the Laplace transform [e.g., Kanasevich (1981)], of the analytical solution given by (2). The Z transform converts a frequency-domain function [say, $A(\omega)$] into Z polynomials [say, $\sum_{k=-\infty}^{\infty} a(k) \cdot z^{-k}$], where $z \equiv e^{i\omega\Delta t}$ and Δt denotes the time sampling interval. The expression z^{-1} can be interpreted as a time delay operator with delay Δt . Taking the Z transform of a frequency-domain function is equivalent to expanding the function using the basis of $z \equiv e^{i\omega n \Delta t}$, where $n = -\infty, \dots, -1, 0, 1, \dots, \infty$. Appendix I is provided to demonstrate the procedure of performing the Z transform. Eq. (2) can be written as an equation of Z polynomials

$$u(x_j, z) = E_j(z) \cdot Z[e^{ik_j x_j}] + F_j(z) \cdot Z[e^{-ik_j x_j}] \quad (5a)$$

where

$$E_j(z) = 0.5 \cdot (1 + \alpha_{j-1}) \cdot D_{j-1}^{-1}(z) \cdot E_{j-1}(z) + 0.5 \cdot (1 - \alpha_{j-1}) \cdot D_{j-1}(z) \cdot F_{j-1}(z) \quad (5b)$$

$$F_j(z) = 0.5 \cdot (1 - \alpha_{j-1}) \cdot D_{j-1}^{-1}(z) \cdot E_{j-1}(z) + 0.5 \cdot (1 + \alpha_{j-1}) \cdot D_{j-1}(z) \cdot F_{j-1}(z) \quad (5c)$$

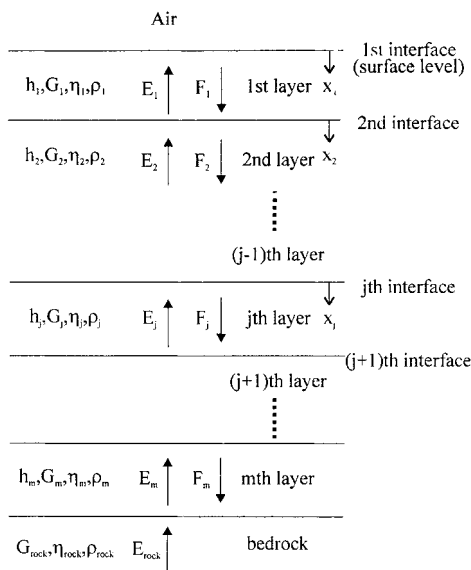


FIG. 1. Hypothetical Horizontal Layered Soil Profile

$$E_{\text{rock}}(z) = 0.5 \cdot (1 + \alpha_m) \cdot D_m^{-1}(z) \cdot E_m(z) + 0.5 \cdot (1 - \alpha_m) \cdot D_m(z) \cdot F_m(z) \quad (5d)$$

$$U_j(z) = E_j(z) + F_j(z) \quad (5e)$$

$$E_1(z) = F_1(z) \quad (5f)$$

$$D_j(z) = Z[e^{-ik_j h_j}] \quad (5g)$$

$$D_j^{-1}(z) = 1/D_j(z) \quad (5h)$$

where $Z[\cdot] = Z$ transform, which creates Z polynomials.

In (5b–d), there are two fundamental mechanisms that act to convert $E_{j-1}(z)$ and $F_{j-1}(z)$ to $E_j(z)$ and $F_j(z)$ (recall that E_j and F_j are the upgoing and downgoing waves, respectively, at the j th interface): (a) The impedance contrast across the j th interface α_{j-1} determines how energy is apportioned to each layer when the wave encounters the j th interface; and (b) the function $D_{j-1}(z)$ determines how the waveform shape changes when traveling in the $(j - 1)$ th layer. For elastic conditions ($\eta = 0$), $D_j(z)$ is just a time-delay operator that does not change the shape of the waveform. The amount of the delay is the travel time of the shear wave in the j th layer [Fig. 2(a)]. In the presence of damping, $D_j(z)$ has the effect of dispersion as well as time delay (Aki and Richards 1980). The more damping, the more the dispersion, as shown in Fig. 2(b–d). The expression $D_j(z)$ is the delay-dispersion operator (DDO) of the j th layer. The DDO is always causal (the coefficients of z^n , $n = -\infty, \dots, -2, -1, 0$, are zero) and transient (the coefficients of z^{-n} , $n = p, p + 1, p + 2, \dots, \infty$ are zero for some p), although the frequency-domain counterpart $e^{-ik_j h_j}$ has been presented as being composed of an infinite series of steady-state (infinite in time) sinusoid functions. The expression $D_j(z)$ can be regarded as the output at the top of the j th soil layer given an impulsive input at the bottom of the j th layer (i.e., an impulse response) in the situation where the j th and $(j + 1)$ th interfaces are absent. The coefficients of $D_j(z)$ depend only on the dynamic mechanical properties and thickness of the j th soil layer and are known as long as the soil profile is available.

To convert (2) to (5), one only needs to perform the Z trans-

form to calculate the DDOs of all soil layers. By knowing the DDOs, $E_j(z)$, $F_j(z)$, and $E_{\text{rock}}(z)$ can be evaluated recursively [(5b–d)] without directly applying the Z transform. The expressions $E_j(z)$, $F_j(z)$, and $E_{\text{rock}}(z)$ can eventually be represented as functions of $E_1(z)$ ($E_1 = F_1$) and the DDOs. The only unknown remaining in (5) is $E_1(z)$. That is to say, the following equation holds:

$$U_j(z) = E_j(z) + F_j(z) = H_j(z) \cdot E_1(z), \quad \text{for all } j \quad (6)$$

where $H_j(z)$ is known Z polynomial whose coefficients depend only on $\alpha_1, \alpha_2, \alpha_3, \dots, \alpha_{j-1}$ and the coefficients of $D_1(z), D_2(z), D_3(z), \dots, D_{j-1}(z)$ —the mechanical properties of the soil layers between the ground surface and j th interface.

The Z -domain transfer function (ZTF) from the i th to k th interface ($i > k$) can be written

$$T_{i-k}(z) = \frac{U_k(z)}{U_i(z)} = \frac{H_k(z) \cdot E_1(z)}{H_i(z) \cdot E_1(z)} = \frac{H_k(z)}{H_i(z)} = \frac{b_1 \cdot z^{-d} + b_2 \cdot z^{-(d+1)} + \dots + b_n \cdot z^{-(d+n-1)}}{1 + a_1 \cdot z^{-1} + a_2 \cdot z^{-2} + \dots + a_m \cdot z^{-m}} \quad (7)$$

where a_1, \dots, a_m = parameters for an infinite impulse response (IIR) filter; and b_1, b_2, \dots, b_n = parameters for a finite impulse response filter. The parameters a_1, a_2, \dots, a_m and b_1, b_2, \dots, b_n depend on the coefficients of $D_1(z), D_2(z), \dots, D_{i-1}(z)$ and $\alpha_1, \alpha_2, \dots, \alpha_{i-1}$ ($i > k$). Both m and n are finite numbers because all DDOs are transient. The value of d is defined as the time delay of the ZTF. Note that the only unknown $E_1(z)$ disappears in (7), so $T_{i-k}(z)$ depends only on the soil properties between the ground surface and i th layer. The properties of soil layers deeper than that are irrelevant. Not surprisingly, $T_{i-k}(z)$ is always causal so long as $i > k$; i.e., the i th interface is deeper than the k th interface. The time delay of $T_{i-k}(z)$ is exactly the travel time of the shear wave from the i th to k th interface.

The final step is to transform (7) to the discrete time domain using the inverse Z transform (recall that z is a time-delay operator with unit delay Δt)

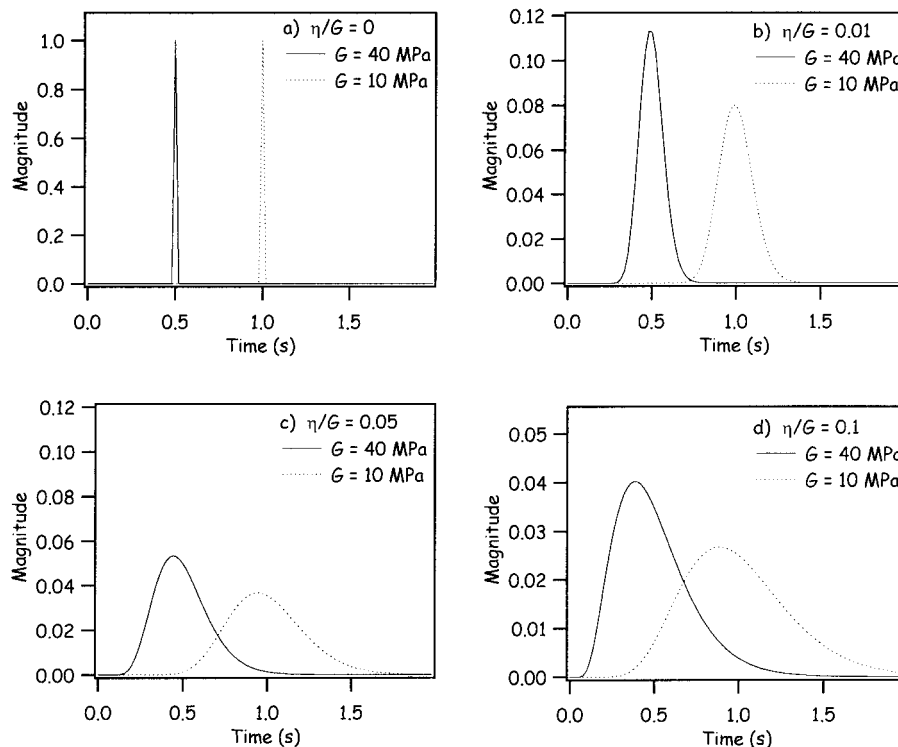


FIG. 2. Comparison of Effect of η/G on Damping-Delay Function for Different Values of G

$$U_k(t) = b_1 \cdot U_i(t-d) + b_2 \cdot U_i(t-d-1) + b_3 \cdot U_i(t-d-2) + \dots + b_n \cdot U_i(t-d-n+1) - a_1 \cdot U_k(t-1) - a_s \cdot U_k(t-2) - a_3 \cdot U_k(t-3) - \dots - a_m \cdot U_k(t-m) \quad (8)$$

where U_i and U_k = displacement time history at the i th and k th interface.

Eq. 8 is the discrete time-domain solution for 1D shear-wave propagation in the form of an IIR filter. Solving for 1D shear-wave propagation now becomes a problem of estimating the filter parameters a and b , which depend on the DDOs and impedance ratio α at each interface. This filter is stable [the roots of $H_i(z)$ in (7) lie outside the unit circle] if η is present in at least one layer and is neutral stable [the roots of $H_i(z)$ in (7) lie to the right on the unit circle] if the η are zero for all layers. Eq. 8 has the advantage of “extracting” the input information from output data. That is, by regressing the output on itself (autoregression), memory of the past states are incorporated into the recursion and shortens the signal duration from which one needs to extract information.

The importance of (8) is that it recasts the close-form solution to (1) as an IIR filter equation. The recursive nature of the IIR equation ensures that both the $H_i(z)$ (numerator) and $H_k(z)$ (denominator) in (7) are short filter series with few parameters to estimate. This greatly simplifies and accelerates the task of predicting ground motions. A typical IIR solution to (7) might have 30 zeroes (numerator) and 40 poles (denominator). For $\Delta t = 0.02$ s, the technique allows prediction of output ground motion at time t using only the input time history from $t - 0.6$ to t s ($30\Delta t$) and output time history from $t - 0.8$ to t s ($40\Delta t$). The rest of the input and output time histories are irrelevant.

In contrast, the traditional methods of predicting output ground motion is to calculate the system transfer function first, then convolve the entire input series with the transfer function. To predict the output at time t , one needs to know the input from $t - T$ to t s, where T is the total duration of the system transfer function. With the traditional method, the system transfer function is the entire $H_i(z)/H_k(z)$, a finite impulse response filter with a very long z polynomial. For a very typical length of 150 poles and 150 zeroes, T must be a full 3 s. Conclusively, the IIR equation allows more rapid prediction of ground motions and this IIR equation has the benefit of being the closed-form solution to (1).

Eq. 8 essentially yields the same solution as Goupillaud's solution (1961) when no damping is present. However, the form of (8) is superior because the assumption that signal travel time in each arbitrary layer is identical is dropped and damping effects are expressly taken into account.

Incorporation of Outcrop Motion, Strain, and Time Derivatives of Displacement

Sometimes it is desirable to evaluate the ZTF from a rock outcrop to the j th interface displacement. This can be done by assuming the rock is purely elastic such that

$$U_{\text{outcrop}}(z) = 2E_{\text{rock}}(z) \cdot z^{-d} \quad (9)$$

Here d denotes the S-wave travel time from the soil-rock interface to the outcrop. The desired ZTF is simply $T_{\text{outcrop}-k}(z) = U_k(z)/U_{\text{outcrop}}(z)$, and an IIR filter similar to (8) will result.

In practice, acceleration time histories are usually used for analyses. The transfer functions for accelerations are identical to the ones for displacements because application of the derivative theorem for the Fourier transform ($i\omega \Leftrightarrow d/dt$) yields (Bracewell 1986)

$$T_{i-k}^{\text{displ}}(z) = Z[T_{i-k}^{\text{displ}}(\omega)] = Z\left[\frac{U_k(\omega)}{U_i(\omega)}\right] = Z\left[\frac{(i\omega)^2 \cdot U_k(\omega)}{(i\omega)^2 \cdot U_i(\omega)}\right] = Z\left[\frac{A_k(\omega)}{A_i(\omega)}\right] = Z[T_{i-k}^{\text{accel}}(\omega)] = T_{i-k}^{\text{displ}}(z) \quad (10)$$

where $A_j(\omega)$ stands for the Fourier transform of the acceleration time history at the j th interface.

For analyzing nonlinear problems involving strain-dependent soil properties, shear strain must be evaluated throughout the profile. It is found that shear strain is related to particle velocity through a similar IIR filter equation

$$\gamma_j(t) = f_0 \cdot \dot{U}_j(t) + f_1 \cdot \dot{U}_j(t-1) + f_2 \cdot \dot{U}_j(t-2) + \dots + f_p \cdot \dot{U}_j(t-p) - e_1 \cdot \gamma_j(t-1) - e_s \cdot \gamma_j(t-2) - e_3 \cdot \gamma_j(t-3) - \dots - e_p \cdot \gamma_j(t-p) \quad (11)$$

where γ_j = shear strain directly beneath the j th interface; and \dot{U}_j = particle velocity at the j th interface. Notice that there is no time delay associated with (11). The detail derivation of (11) is given in Appendix II. After evaluating strain, the discrete time history for stress can be determined by (4). The solutions thus calculated are exact at the sampling points as long as there is no aliasing during the evaluation of the DDOs (see Appendix I for how to avoid aliasing). Spatial discretization and specific time-stepping techniques are not required for the solutions.

Nonlinear G and η

The proposed time-domain solution was derived in part to directly accommodate nonlinear soil properties. Any nonlinear behavior of G and η can be incorporated into this model if the nonlinear relationship itself does not change through time; i.e., the modulus degradation curve of a given soil is not a time-dependent property. Time-domain solutions compute responses with time as the direct variable, so it is possible to incorporate past behavior (history) into the computation of the present state.

For simplicity, the nonlinear analysis is carried out using the well-known equivalent-linear approach. That is to say, one assumes $G_j(x_j, t)$ and $\eta_j(x_j, t)$ (x_j is the local coordinate of the j th layer, and $G_j(x_j, t)$ and $\eta_j(x_j, t)$ are the values of G and η of the soil element at x_j and time instant t) are functions of $\gamma_j(x_j, t)$ (the shear-strain level of the soil element at x_j and time instant t). Starting from the first segment ($t = 1$), the values of $G_j(x_j, t)$, $\eta_j(x_j, t)$, and $\gamma_j(x_j, t)$ of each soil layer are updated through time; $G_j(x_j, t)$ and $\eta_j(x_j, t)$ are calculated based on the value of $\gamma_j(x_j, t-1)$ through degradation curves. The value of $\gamma_j(x_j, t)$ of a given soil layer at any fixed time step is never uniform throughout—it varies with depth, as do $G_j(x_j, t)$ and $\eta_j(x_j, t)$. The average G and η (with respect to the thickness of that soil layer) of the j th layer at time instant t can be calculated by the following equation:

$$\frac{h_j}{\sqrt{\rho_j/[G_j(t) + i\omega\eta_j(t)]}} = \int_{h_j} \frac{1}{\sqrt{\rho_j/[G_j(x_j, t) + i\omega\eta_j(x_j, t)]}} dx_j \quad (12)$$

where $\underline{G}_j(t)$ and $\underline{\eta}_j(t)$ = average G and η of the j th layer at time instant t . This equation ensures that $\underline{G}_j(t)$ and $\underline{\eta}_j(t)$ result in the same DDO as using $G_j(x_j, t)$ and $\eta_j(x_j, t)$, while x_j varies from 0 to h_j . In the case where $\eta_j/G_j \ll 1$, one can equate the real and imaginary parts of (12) to get the following equations:

$$\underline{G}_j(t) \approx \left[\frac{1}{h_j} \int_{h_j} \sqrt{G_j(x_j, t)} dx_j \right]^2 \quad (13a)$$

$$\underline{\eta}_j(t) \approx \left[\frac{1}{h_j} \int_{h_j} \frac{\eta_j(x_j, t)}{\sqrt{G_j(x_j, t)}} dx_j \right] \cdot \sqrt{\underline{G}_j(t)} \quad (13b)$$

It is not computationally economical to calculate $G_j(x_j, t)$ and $\eta_j(x_j, t)$ throughout the entire thickness h_j , so Gauss integration (Conte and de Boor 1980) is quite helpful for computing these integrals. By adding interfaces at the Gauss integration points, $\gamma_j(x_j, t - 1)$ at the Gauss points can be calculated using (11), and $G_j(x_j, t)$ and $\eta_j(x_j, t)$ can be evaluated at these points. Eq. 13 can then be employed to compute $G_j(t)$ and $\eta_j(t)$ numerically, and the "linear" transfer functions at time t are computed based on $\underline{G}_j(t)$ and $\underline{\eta}_j(t)$. Given the transfer functions, the resulting responses of the soil system at the gauss points are calculated and $\gamma_j(x_j, t)$ is updated accordingly. With $\gamma_j(x_j, t)$ calculated at the Gauss points, $\underline{G}_j(t + 1)$ and $\underline{\eta}_j(t + 1)$ can be updated and the entire procedure is repeated for the next step.

It is important to recognize that the shear-strain level used to calculate G and η should not be the instantaneous shear strain. It is more reasonable to use the envelope of the shear-strain time history, which can be computed by the Hilbert transform technique (Bracewell 1986). For the nonlinear analysis, simple forward time stepping is all that is necessary, because the transfer functions calculated from (7) are always stable. The entire scheme, therefore, is always stable. For completeness, the solution of a Runge-Katta Rank 4 scheme (Conte and de Boor 1980) was compared to this solution for several test cases. The differences were insignificant.

CASE STUDIES

An especially potent tool for validating the time-domain model is the blind prediction of strong motions recorded at vertical seismic arrays. For these sites, the predicted motions at various points in the soil profile can be directly compared to actual displacement or acceleration time history, using actual at-depth input data. Two sites with vertical arrays, Garner Valley, and Wildlife in Imperial Valley, Calif., were examined for this paper.

Both cases will be analyzed using displacement time histories, because the lower frequency displacement histories are much simpler waveforms to the eye, so the predicted and observed time histories can be more readily compared in detail. As demonstrated by (10), the analyses of displacement and acceleration are equivalent because their transfer functions are actually the same. All displacement datum were yielded by double integration of acceleration and high pass filtering at 0.2 Hz using a fourth-order Butterworth filter.

Throughout the case studies, the term "damping ratio" is avoided. Instead, η/G is defined to be a measurement of dispersion. Based on (3), η/G is approximately equivalent to the damping ratio for the practical range of predominant frequencies of displacement time history and commonly accepted values for β are used for η/G .

Garner Valley

For the case of Garner Valley, the soil profile and locations of the accelerometers are shown in Fig. 3 (Archuleta et al. 1992). Five accelerometers are located at 0, 15, 22, 55, and 220 m depth. The shear-wave velocities, soil densities, and soil type are known in detail to a depth of 90 m (Nigbor and Steller 1996). The shear-wave velocities and densities of the soils deeper than 90 m are assigned with reasonable values given by Archuleta et al. (1992).

As an example, the Joshua Tree earthquake [April 23, 1992, Magnitude (M) 6.1, PGA = 0.1 g] analysis will be presented. Both linear and nonlinear analyses were implemented for the purpose of comparison. For the linear analysis, all G and η are assumed to remain constant during the earthquake. The values of G are estimated from the shear-wave velocities shown on the soil profile in Fig. 3, and $\eta/G \cong \beta$ are assumed

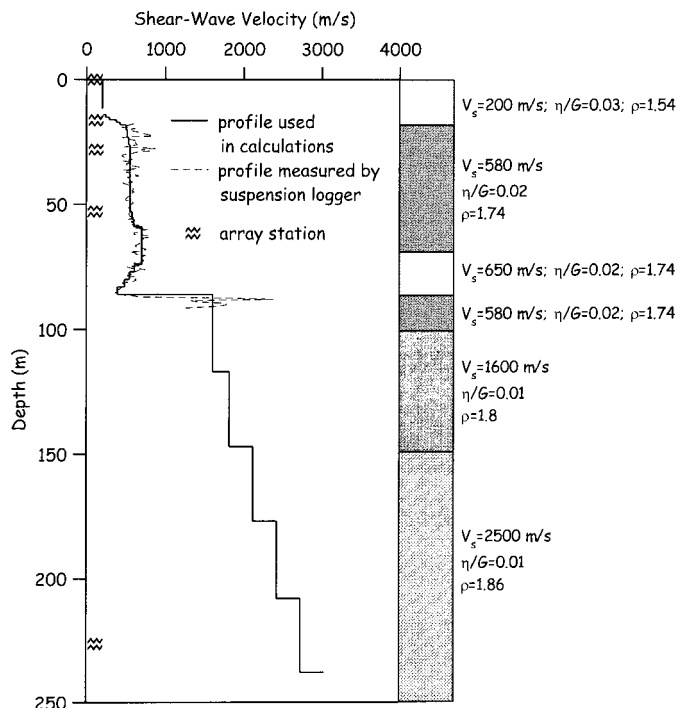


FIG. 3. Soil Profile and Material Properties for GVDA (Archuleta et al. 1992; Nigbor and Steller 1996)

TABLE 1. Soil Parameters and Degradation Curves Used for GVDA Analyses

| Depth (m) (1) | G/G_{max} versus shear strain (2) | η/G_{max} versus shear strain (3) |
|---------------|---|--|
| 0 ~ 4.5 | $PI = 0, OCR = 1-15$ (Vucetic and Dobry 1991) | $PI = 0, OCR = 1-8$ (Vucetic and Dobry 1991) |
| 4.5 ~ 14.5 | Sand $\sigma_v = 1-3$ ksf (Sun et al. 1988) | Average sand (Seed and Idriss 1970) |
| 14.5 ~ 18 | Sand $\sigma_v > 3$ ksf (Sun et al. 1988) | Average sand (Seed and Idriss 1970) |
| 18 ~ 220 | $PI = 15, OCR = 1-15$ (Vucetic and Dobry 1991) | $PI = 15, OCR = 1-8$ (Vucetic and Dobry 1991) |

reasonable values, as shown in Fig. 3. For nonlinear analyses the degradation curves of each soil layer are listed in Table 1. As a further comparison, estimates were also made using SHAKE.

The records at 0, 15, 22, 55, and 220 m depth were studied in pairs: while the displacement time history at 220 m was set as input, the output (predicted) time histories at 55 m were compared to the actual record and so forth for 55-22 m, 22-15 m, 15-m-surface level, and entire 220-m-surface level soil columns.

The predicted and observed surface ground motions for each pair are compared in Fig. 4. The difference between the linear and nonlinear analyses is extremely small. The effect of different values of damping (η/G varying from 0.01 to 0.1) was also found to be negligible for these solutions. For direct comparison, the surface ground motions predicted by SHAKE, using identical input data, is contrasted in Fig. 5 to the actual and time-domain estimate. Although the thin interval estimates (e.g., 15-m-surface, 22-15 m, and 55-22 m pairs) are relatively accurate, the estimates for thicker profiles, especially the 220-m-surface and 220-55 m estimates in Fig. 5, show discrepancies compared to the actual observed time histories. SHAKE overestimates the amplitudes of the ground motions for the two pairs.

The studies of two other earthquakes (May 4, 1992, M 4.1, PGA = 0.01g and July 7, 1992, M 5.0, PGA = 0.02g) lead to

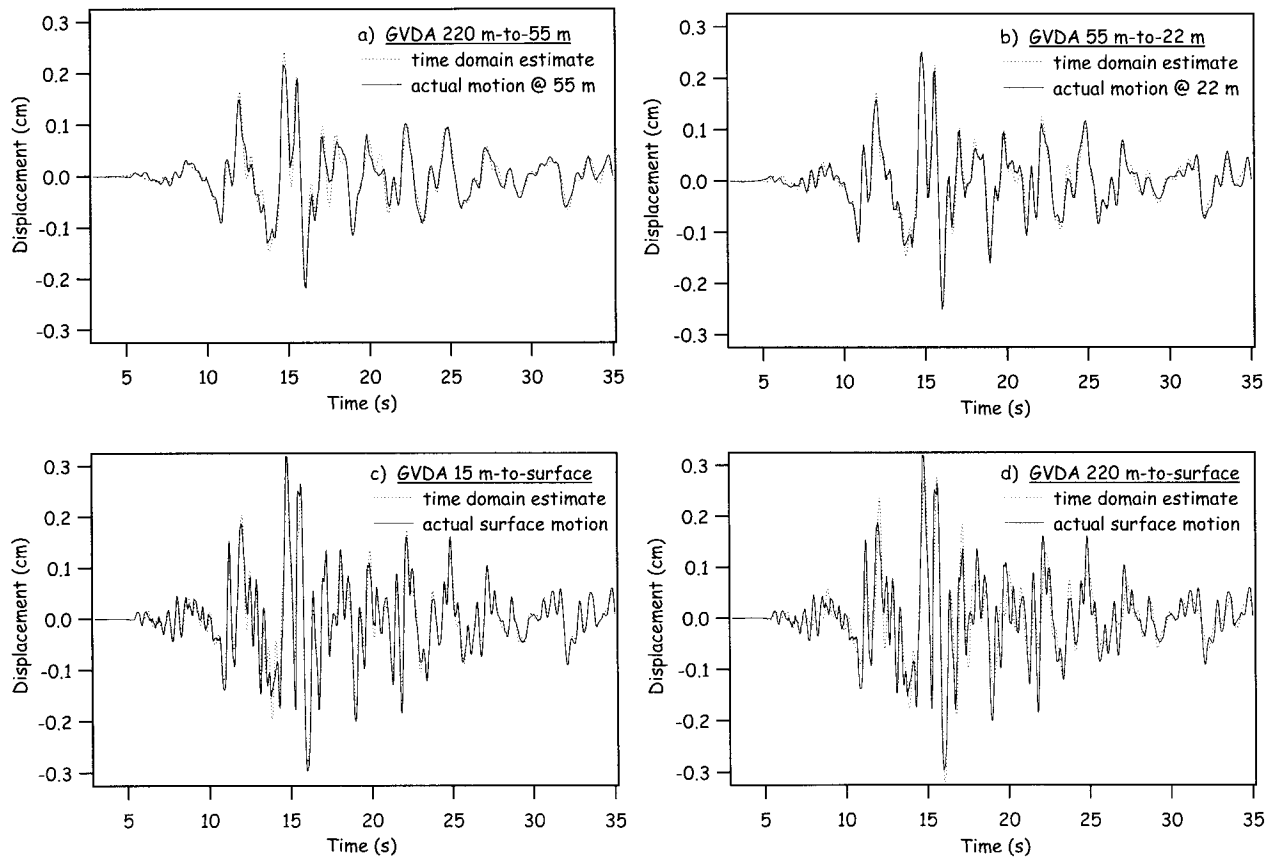


FIG. 4. Comparison of Time-Domain Predicted Ground Motions and Actual Recorded Ground Motions for GVDA: (a) 220–55 m; (b) 55–22 m; (c) 15-m–Surface; (d) 220-m–Surface

the same conclusions as drawn from the Joshua Tree earthquake. The time-domain solution yields satisfactory predictions for all pairs, whereas SHAKE predicts the thin intervals well but overestimates the amplitudes for thicker intervals. SHAKE also overestimates the pair involving the 55-m record for the M 5.0 event and the 15, 22, and 55 m records for the M 4.1 event. Figs. 6 and 7 show the predictions of the time-domain solution and SHAKE for the 15-m–surface interval of the M 4.1 event and the 55-m–surface interval of the M 5.0 events, respectively. The studies of all other intervals deeper than these show the same overestimation by SHAKE.

The following two trends apply to all vertical array records analyzed (including the other nine events for the Garner Valley site and several events for the Chiba site in Japan, which are not shown in this paper for space considerations): (a) The deeper the vertical array interval, the more likely that SHAKE overestimates the ground motions and the more exaggeration SHAKE predicts; and (b) the smaller the earthquake, the more likely the overestimates extend to the shallower intervals. The time-domain solution is immune to the two conditions and yields good predictions for most cases.

Wildlife Site

The Wildlife site was strongly shaken on November 23–24, 1987 by two earthquakes, Elmore Ranch (M_s 6.2) and Superstition Hills (M_s 6.6). The site liquefied during the latter temblor and was monitored by a vertical array operating onsite (Holzer et al. 1989a), allowing a direct comparison of linear and nonlinear behavior of a single site. The soil profile and position of accelerometers and piezometers is shown in Fig. 8 (Bennett et al. 1984; Haag 1985), and soil parameters and degradation curves are listed in Table 2. For the analysis of both temblors, the displacement time history at the lower (7.5-m) accelerometer was used as input to the system. The pre-

dicted and observed time histories at the surface level were then compared.

For the Elmore Ranch earthquake, one assumes G and η did not vary over time (i.e., linear analysis) and reasonable values of $\eta/G \approx \beta$ for each layer were used, as given in Fig. 8. The predicted and observed ground motions at the surface are compared in Fig. 9; the predictions match the actual ground motions accurately.

For the Superstition Hills earthquake, liquefaction was believed to have started in the B1 sublayer (2.5–3.5 m) and migrated downward through the B2 horizon, as indicated by the recorded pore-pressure records (Holzer et al. 1989b). For this situation, both G and η of these layers are expected to vary significantly. To facilitate comparison between linear and nonlinear methodologies, the same IIR filter parameters from the Elmore Ranch earthquake (constant G and η) were used for first-order prediction of the displacement time history at the ground level for the 360° component records of the Superstition Hills earthquake. As shown in Fig. 10, the linear estimate quality was good before approximately $T = 13$ s, which corresponds to the time of rapid pore-pressure buildup (Glaser 1996). With the pore-pressure buildup at 13 s, the calculated displacement started to diverge from the actual time history. Moreover, the time delays between predicted and observed peaks became longer with time, indicating that the soils were progressively weakening and behaving highly nonlinearly.

DISCUSSION

Use of Ideal Hysteretic Damping Model

From the results of the case studies, it was found that in some situations SHAKE cannot predict time histories accurately. The linear time-domain solution solves the same gov-

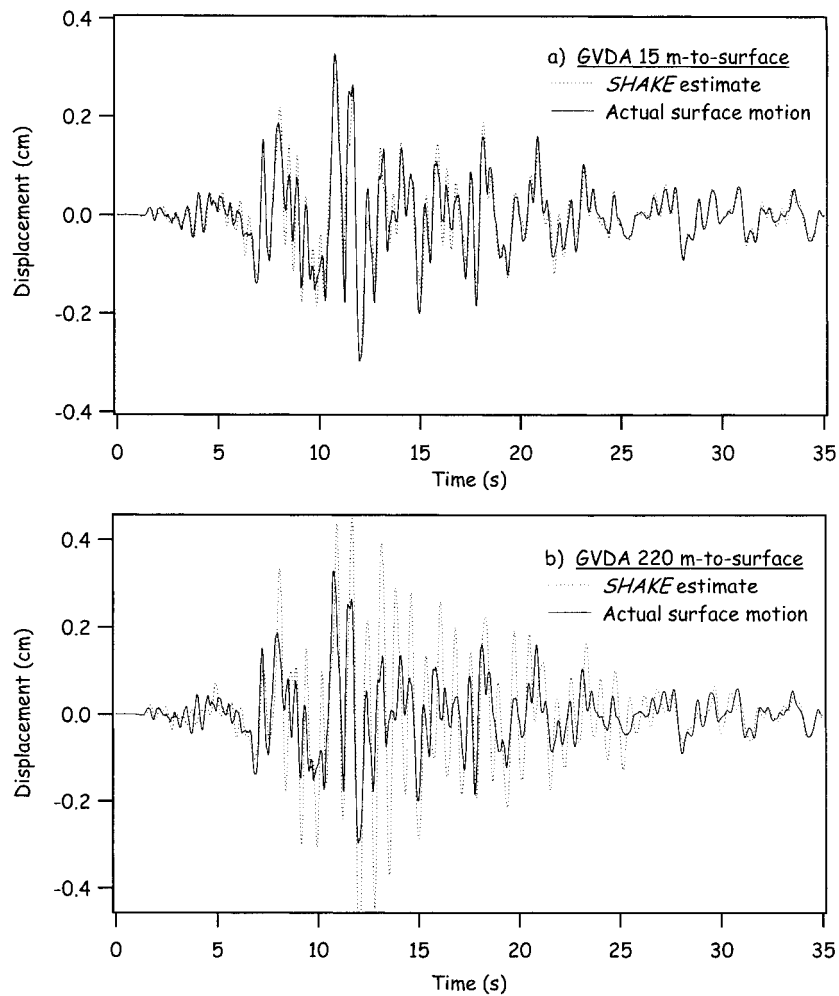


FIG. 5. Comparison of SHAKE Predicted Ground Motions and Actual Recorded Ground Motions for GVDA: (a) Thin Layer, 15-m-Surface; (b) Thick Layer, 220-m-Surface

erning equation [(1)] as SHAKE but always yields good results as long as the soil remains a solid. The two differences between this approach and SHAKE are (a) SHAKE uses the hysteretic damping model whereas the time-domain solution assumes viscous damping; and (b) SHAKE solves the problem in the frequency domain whereas the time-domain solution solves it in the time domain.

SHAKE uses the hysteretic damping model because G and β are believed to be frequency independent. Unfortunately, the SHAKE formulation of hysteretic damping is not appropriate. Eq. 3 can be written equivalently

$$\tau(\omega) = [G + 2i\beta] \cdot \gamma(\omega) \quad (14a)$$

or simply

$$\tau(t) = [G + 2i\beta] \cdot \gamma(t) \quad (14b)$$

which states that a real-valued $\gamma(t)$ results in a complex-valued $\tau(t)$, which violates physical laws. This physical difficulty can be corrected by rewriting Eq. 14 (Inaudi and Kelly 1995)

$$\tau(\omega) = [G + 2i\beta \cdot \text{sgn}(\omega)] \cdot \gamma(\omega) \quad (15)$$

where $\text{sgn}(\omega) = 1$ if $\omega > 0$, -1 if $\omega < 0$, and 0 if $\omega = 0$.

Replacing (3) with (5) does not solve all problems. The ideal linear hysteretic damping model [(15)], characterized by frequency-independent G and β , is inherently noncausal (Crandall 1963; Inaudi and Kelly 1995; Inaudi and Makris 1996). This noncausality makes it difficult to write (15) in the time domain, because for a causal system the real and imag-

inary parts of its frequency response must be related through the Hilbert transform (Aki and Richards 1980). Eq. (15), however, does not ensure this. The noncausality of the ideal hysteretic damping model also results in noncausal DDOs. In contrast, the DDOs resulting from the viscous damping model are always causal, as shown in Fig. 2.

Another major difference between the two damping models concerns the predicted spectral ratios. Fig. 11 illustrates the spectral ratios predicted by the time-domain solution and SHAKE for the 15-m-surface and 200-m-surface pairs of the Garner Valley case study. Also shown in the figure are the spectra of the input motions. For the viscous damping model (presented here), the amplitude of the first mode is smaller and the higher frequency modes have much smaller participation. For the hysteretic damping model, the first mode amplitude is high and strong participation of many higher modes are estimated. Despite differences between the two models, the predicted spectral ratios are approximately the same in the frequency range below the first natural mode (3.26 Hz for the 15-m-surface pair and 1.4 Hz for the 220-m-surface pair). However, the first mode of the 220-m-surface pair transfer function is close to the main energy range of the input motion. This is possibly the direct cause of the overestimation by SHAKE for the 220-m-surface pair.

Effects of Dispersion and Nonlinearity

As shown in the case studies, the viscous damping coefficient η does not appear to have significant effects on predicted ground motions. One possible explanation is that very thick

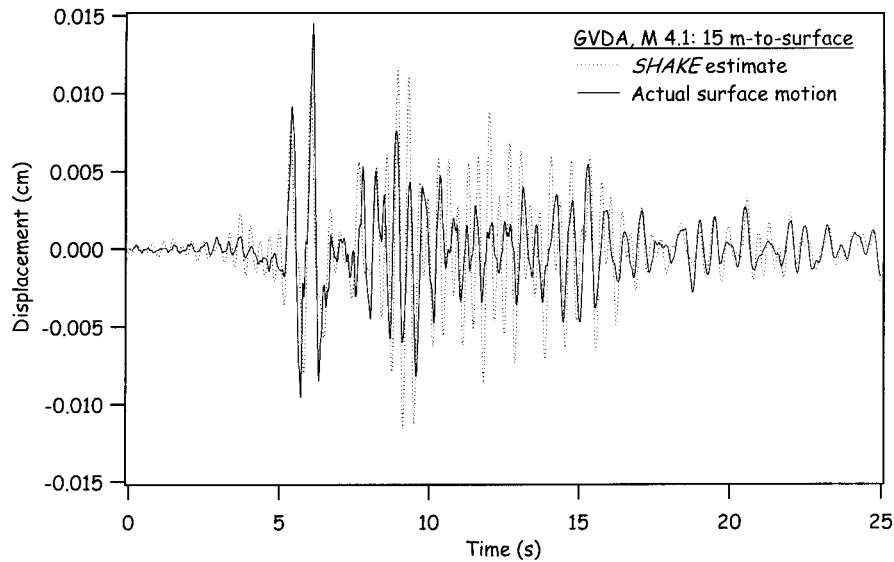


FIG. 6. Comparison of Actual, and SHAKE Estimates for Ground Motions, for Thick Layer, for GVDA M 4.1, and 15-m-Surface

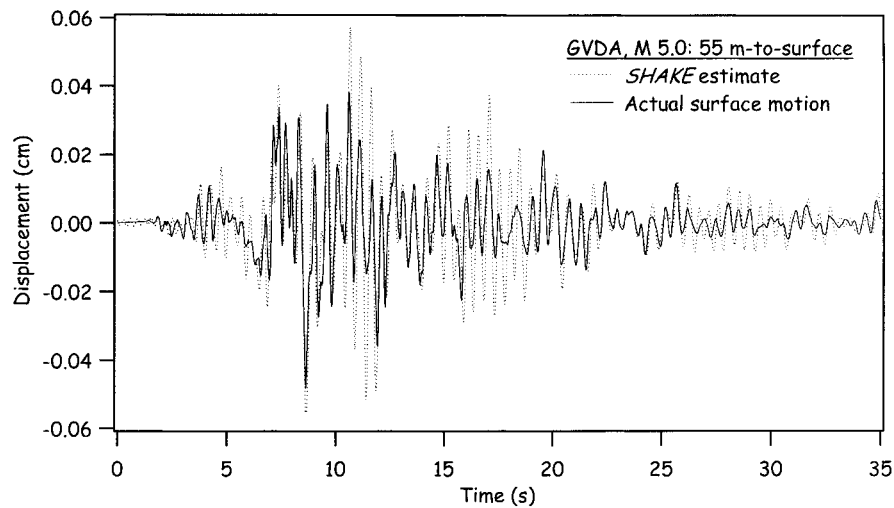


FIG. 7. Comparison of Actual, and SHAKE Estimates for Ground Motions, for Thin Layer, for GVDA M 5.0, and 55-m-Surface

soil layers are required for η to have a significant effect. For a lightly damped soil, if the dominant wavelength of the earthquake is much larger than the layer thickness, η has virtually no effect on the waveform. For instance, the average V_s of the top 55-m soils of the Garner Valley site is about 200 m/s. Assuming the predominant period is 3 s, the corresponding wavelength is 600 m, which is much larger than the soil thickness of 55 m. As a result, the damping coefficient does not play a significant role in the behavior. Another interpretation is that DDOs actually act as low-pass filters. The thicker the soil layer, the lower the filter cutoff frequency. If one has a thin layer, the layer acts like a low-pass filter with a high cutoff frequency, hence having no effect from low frequency earthquake motions.

For all but the most extreme cases, it was found that linear predictions were as accurate as nonlinear, even for the case of high intensity ground motion. The only exception was the Wildlife site where soils liquefied during the Superstition Hills temblor. In this case, it is very likely that liquefied soils behave significantly different from normal soils, such that (1) is no longer a reasonable model to capture the dynamics.

CONCLUSIONS

An equivalent-linear time-domain solution for predicting earthquake ground motion based on the 1D shear-wave equation with a viscous damping model has been developed. The solution of the time-domain model has several advantages including causality, direct modeling of impulsive and transient processes, and ease of inclusion of nonlinear soil behavior. The presented derivation results in a stable infinite impulse response filter equation in the time domain and only needs soil shear-wave velocity, density, and damping coefficient profiles to characterize the soil.

Several case studies were presented that show that blind prediction of surface (and interval) ground motion is virtually identical to that measured. This was shown using strong motion records from the Garner Valley and Wildlife site vertical arrays, which give an actual layer-by-layer time history against which to judge the behavior of this model. For an earthquake large enough to cause liquefaction (1987 Superstition Hills event at the Wildlife site), the degree of fit between actual and estimated response made using a linear model is good up to the onset of liquefaction.

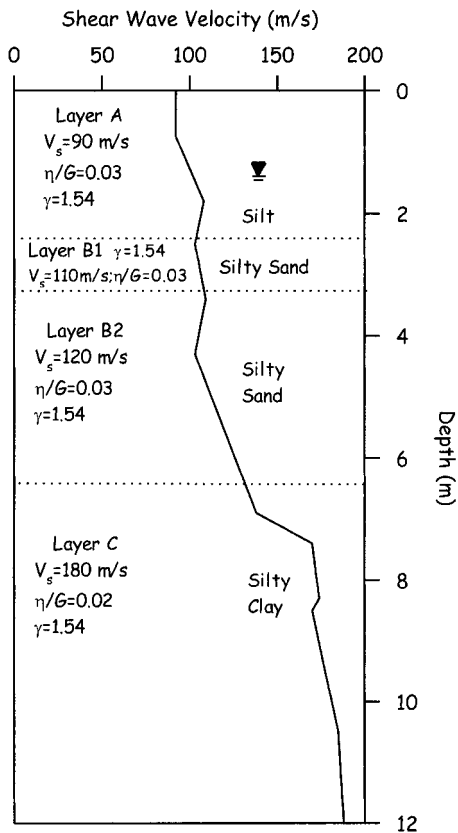


FIG. 8. Soil Profile and Physical Properties for Wildlife Site

TABLE 2. Soil Parameters and Degradation Curves Used for Wildlife Site Analyses

| Depth (m) (1) | G/G_{max} versus shear strain (2) | η/G_{max} versus shear strain (3) |
|---------------|---|--|
| 0 ~ 6.5 | $PI = 0, OCR = 1-15$ (Vucetic and Dobry 1991) | $PI = 0, OCR = 1-8$ (Vucetic and Dobry 1991) |
| 6.50 ~ 12 | $PI = 15, OCR = 1-15$ (Vucetic and Dobry 1991) | $PI = 15, OCR = 1-8$ (Vucetic and Dobry 1991) |

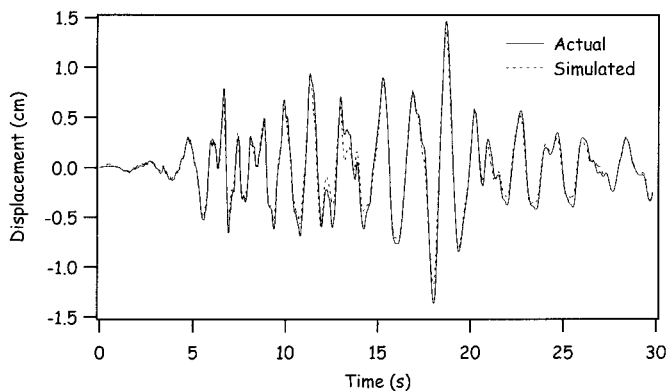


FIG. 9. Comparison of Simulated Elmore Ranch Earthquake Surface Motion to Actual Motion

In comparison, SHAKE does not in some situations provide satisfactory predictions of the time histories of ground motions. Previous work shows that the hysteretic damping model used by SHAKE is not physically realizable (Inaudi and Kelly 1995; Inaudi and Makris 1996). From the results of the case studies, SHAKE overpredicts the amplification at the first and higher modes.

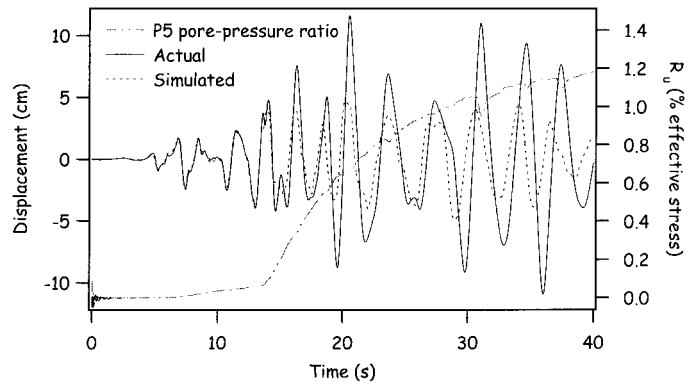


FIG. 10. Comparison of Superstition Hills Surface Motions Simulated with Linear Elmore Ranch Model to Actual Motions (Pore-Water Pressure Ratio for Piezometer P5 Is Shown to Indicate Relationship between Softening and Pore Pressure)

APPENDIX I. Z TRANSFORM OF ANALYTIC FREQUENCY-DOMAIN FUNCTION $A(\omega)$

The purpose of this appendix is to demonstrate how to convert a frequency-domain function $A(\omega)$ to the corresponding Z polynomials $A(z)$; that is, to find $a(k)$ such that

$$A(\omega) = \sum_{k=-\infty}^{\infty} a(k) \cdot e^{-i\omega \cdot dt \cdot k} = \sum_{k=-\infty}^{\infty} a(k) \cdot z^k \equiv A(z) \quad (16a)$$

whereas $a(k)$ = coefficients of the Z polynomials $A(z)$. The value of $a(k)$ can be evaluated by use of the Fourier integral

$$a(k) = \left(\frac{1}{2\pi} \right) \cdot \int_0^{2\pi/dt} A(\omega) \cdot e^{i\omega \cdot dt \cdot k} d\omega \quad (16b)$$

where $a(k)$ can also be interpreted as the discrete-time-domain incarnation of $A(\omega)$. Notice that (16a) assumes that $A(\omega) = A(\omega + 2\pi/dt)$, or $A(\omega)$ is periodic with period $2\pi/dt$. Frequency-domain aliasing could occur if $A(\omega)$ is not band-limited within $\omega = \pi/dt$, the Nyquist frequency. Fortunately, the damping-delay function $D_j(\omega) = e^{-k_j/\eta_j}$ can always be made band limited at the Nyquist frequency by decreasing dt (i.e., increasing the Nyquist frequency) if the damping term η is present. So frequency-domain aliasing is not an issue in evaluating $D_j(z)$.

Computing $g(k)$ by the Fourier integral [(16b)] is not a trivial task. To make the computation of $a(k)$ feasible, the function $B(\omega)$ is introduced

$$B(\omega) = \sum_{n=-\infty}^{\infty} \delta \left(\omega - \frac{2\pi n}{N \cdot dt} \right) \quad (17)$$

where N = desired number of $a(k)$, the coefficients of $A(z)$; δ = Dirac delta function; and $B(\omega)$ can be regarded as a frequency-domain sampling function with a sampling interval of $2\pi/(N \cdot dt)$. Because $B(\omega)$ is also a periodic function with a period of $2\pi/dt$, it can be rewritten

$$B(\omega) = \sum_{k=-\infty}^{\infty} b(k) \cdot e^{-i\omega \cdot dt \cdot k} \quad (18a)$$

where

$$\begin{aligned} b(k) &= \left(\frac{1}{2\pi} \right) \cdot \int_0^{2\pi/dt} \sum_{n=-\infty}^{\infty} \delta \left(\omega - \frac{2\pi n}{N \cdot dt} \right) \cdot e^{i\omega \cdot dt \cdot k} d\omega \\ &= \left(\frac{1}{2\pi} \right) \cdot \sum_{n=0}^{N-1} e^{i2\pi nk/N} \end{aligned} \quad (18b)$$

Based on the inverse discrete Fourier transform, $b(k)$ is

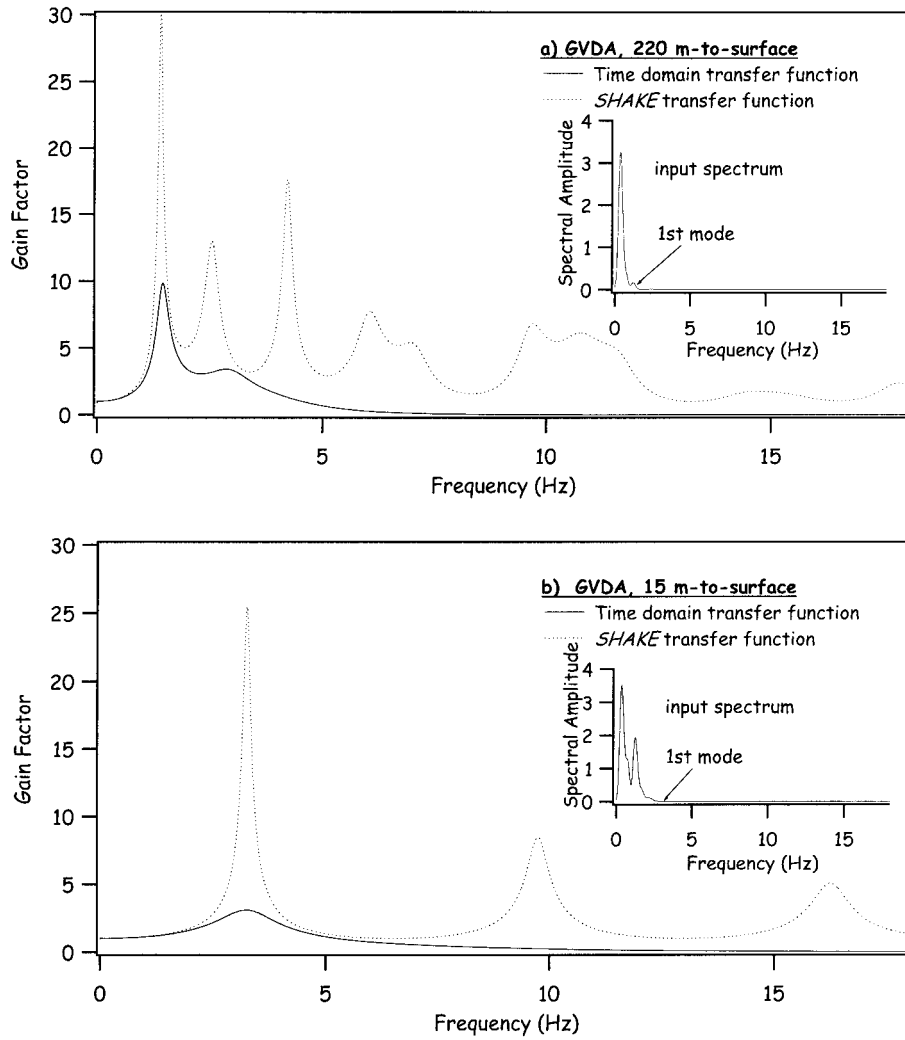


FIG. 11. Comparison of Time-Domain and SHAKE Calculated Transfer Functions, with Input Motions Shown: (a) Poor SHAKE Performance for Thick (220-m) Layer; (b) Good SHAKE Performance for Thin (15-m) Layer

$$b(k) = \begin{cases} \frac{N}{2\pi}, & k = 0, \pm N, \pm 2N, \dots \\ 0, & \text{otherwise} \end{cases} \quad (19)$$

where $b(k)$ can also be interpreted as the discrete-time-domain function of $B(\omega)$.

According to the convolution principal

$$a(k) \otimes b(k) = F^{-1}[A(\omega) \cdot B(\omega)] \quad (20a)$$

$$a(k) \otimes b(k) = \left(\frac{1}{2\pi}\right) \cdot \int_0^{2\pi/dt} A(\omega) \cdot B(\omega) \cdot e^{i\omega \cdot dt \cdot k} d\omega \quad (20b)$$

$$a(k) \otimes b(k) = \left(\frac{1}{2\pi}\right) \cdot \int_0^{2\pi/dt} \sum_{n=-\infty}^{\infty} \delta\left(\omega - \frac{2\pi n}{N \cdot dt}\right) \cdot A(\omega) \cdot e^{i\omega \cdot dt \cdot k} d\omega \quad (20c)$$

$$a(k) \otimes b(k) = \left(\frac{1}{2\pi}\right) \cdot \sum_{n=0}^{N-1} A\left(\omega = \frac{2\pi n}{N \cdot dt}\right) \cdot e^{i2\pi nk/N} \quad (20d)$$

where \otimes = discrete-time-domain convolution operator. Eq. (20) states that $a(k) \otimes b(k)$ is the inverse discrete Fourier transform of sampled $A(\omega)$. Notice that $a(k) \otimes b(k)$ is a periodic function of period N with repeated $a(k)$. If $a(k) = 0$ for all $k \geq N$ [i.e., no time-domain aliasing, or transient signals, otherwise it is not possible to recover $a(k)$], one can rewrite (20) as

$$a(k) = \left(\frac{1}{N}\right) \cdot \sum_{n=0}^{N-1} A\left(\omega = \frac{2\pi n}{N \cdot dt}\right) \cdot e^{i2\pi nk/N} \quad (21)$$

for k between 0 and $N - 1$. Time-domain aliasing is not an issue for the damping-delay functions because they can always be made transient within N if N is large enough. The selection of N depends on how fast the $a(k)$ converge to zero. For instance, it is appropriate to let N be 50 for the solid line in Fig. 2(b). After the $a(k)$ are evaluated, the Z polynomials $A(z)$ are ready to be calculated by (16a).

In summary, the evaluation of $A(z)$ from $A(\omega)$ involves three steps: (1) Transforming from the continuous frequency domain to the discrete domain $A(\omega = 2\pi n/Ndt)$, where $n = 0 \sim (N - 1)$ —(make sure that $A(\omega)$ is band-limited within π/dt); (2) compute $a(k) = \sum_{n=0}^{N-1} A(\omega = 2\pi n/Ndt) \cdot e^{i2\pi nk/N}$ (make sure that $a(k) = 0$ for all $k \geq N$); and (3) the Z polynomials $A(z)$ are set to be $\sum_{k=0}^{N-1} a(k) \cdot z^{-k}$.

APPENDIX II. EVALUATION OF SHEAR STRAIN

To evaluate shear strain, return to the frequency-domain equation [(2a)] and take the spatial derivative with respect to x_j , the local coordinate

$$\gamma(x_j, \omega) = \partial u(x_j, \omega) / \partial x_j = ik_j(\omega) \{E_j(\omega) \cdot e^{ik_j x_j} - F_j(\omega) \cdot e^{-ik_j x_j}\} \quad (22a)$$

$$\gamma(x_j, \omega) = i\omega \sqrt{\rho_j / (G_j + i\omega\eta_j)} \cdot \{E_j(\omega) \cdot e^{ik_j x_j} - F_j(\omega) \cdot e^{-ik_j x_j}\} \quad (22b)$$

Because the value of $\omega \cdot \eta$ is much less than G for most soils and rocks in the frequency range of interest, the function

$\sqrt{\rho_j/(G_j + i\omega\eta_j)}$ is weakly dependent on frequency and can be replaced by $1/V_j$ without significant error, where V_j is the shear-wave velocity of the j th layer. At the point directly beneath the j th interface [set $x_j = 0$ in (12)], the strain is

$$\gamma_j(\omega) = i\omega\sqrt{\rho_j/(G_j + i\omega\eta_j)} \cdot [E_j(\omega) - F_j(\omega)] \quad (23a)$$

$$\gamma_j(\omega) \approx i\omega(1/V_j) \cdot [E_j(\omega) - F_j(\omega)] \quad (23b)$$

$$\gamma_j(\omega) = (i\omega/V_j) \cdot [E_j(\omega) + F_j(\omega)] \cdot \{[E_j(\omega) - F_j(\omega)]/[E_j(\omega) + F_j(\omega)]\} \quad (23c)$$

$$\gamma_j(\omega) = (i\omega/V_j) \cdot U_j(\omega) \cdot \{[E_j(\omega) - F_j(\omega)]/[E_j(\omega) + F_j(\omega)]\} \quad (23d)$$

One now has the required equation in the Z domain

$$\begin{aligned} \gamma_j(z) &= (1/V_j) \cdot \left[\frac{E_j(z) - F_j(z)}{E_j(z) + F_j(z)} \right] \cdot \dot{U}_j(z) \\ &= \frac{f_0 + f_1 \cdot z^{-1} + f_2 \cdot z^{-2} + \dots + f_p \cdot z^{-p}}{1 + e_1 \cdot z^{-1} + e_2 \cdot z^{-2} + \dots + e_p \cdot z^{-p}} \cdot U_j^*(z) \end{aligned} \quad (24)$$

where $\dot{U}_j(z) = Z$ -domain function of the velocity time history at the j th interface; and e_i and f_i are the filter coefficients depending on the coefficients of $D_1(z)$, $D_2(z)$, \dots , $D_{j-1}(z)$ and $\alpha_1, \alpha_2, \dots, \alpha_{j-1}$.

The discrete time-domain equation for strain is

$$\begin{aligned} \gamma_j(t) &= f_0 \cdot \dot{U}_j(t) + f_1 \cdot \dot{U}_j(t-1) + f_2 \cdot \dot{U}_j(t-2) + \dots \\ &+ f_p \cdot \dot{U}_j(t-p) - e_1 \cdot \gamma_j(t-1) - e_2 \cdot \gamma_j(t-2) \\ &- e_3 \cdot \gamma_j(t-3) - \dots - e_p \cdot \gamma_j(t-p) \end{aligned} \quad (25)$$

ACKNOWLEDGMENTS

This research has been supported by the National Science Foundation, Washington, D.C., Grant No. CMS-9727002. Additional funding from PG&E/PEER is also appreciated. Special thanks go to Ralph Archuleta, Robert Nigbor, and the USGS for supplying much needed data. The writers also want to thank Adrian Rodriguez-Marek for performing the SHAKE analyses, Raymond Seed for his review of the SHAKE results, and Nicholas Sitar for his excellent review and recommendations.

APPENDIX III. REFERENCES

- Aki, K., and Richards, P. G. (1980). *Quantitative seismology*, Freeman, San Francisco.
- Archuleta, R. J., Seale, S. H., Sangas, P. V., Baker, L. M., and Swain, S. T. (1992). "Garner Valley down hole array of accelerometers: Instrumentation and preliminary data analysis." *Bull. Seismological Soc. of Am.*, 82(4), 1592–1621.
- Bennett, M. J., McLaughlin, P. V., Sarmiento, J. S., and Youd, T. L. (1984). "Geotechnical investigation of liquefaction sites, Imperial Valley, California." *Open File Rep. 84-252*, U.S. Geological Survey, Menlo Park, Calif.
- Borja, R. I., Lin, C. H., Sama, K. M., and Masada, G. M. (2000). "Modeling non-linear ground response of non-liquefiable soils." *Earthquake Engrg. and Struct. Dyn.*, 29(1), 63–83.
- Bracewell, R. N. (1986). *The Fourier transform and its applications*, 2nd Ed., McGraw-Hill, New York.
- Claerbout, J. F. (1968). "Synthesis of a layered medium from its acoustic transmission response." *Geophysics*, 33, 264–269.
- Conte, S. D., and de Boor, C. (1980). *Elementary numerical analysis*, 3rd Ed., McGraw-Hill, New York.
- Crandall, S. H. (1963). "Dynamic response of systems with structural damping." *Air, space and instruments, Draper anniversary volume*, McGraw-Hill, New York.
- Crandall, S. H. (1991). "The hysteretic damping model in vibration theory." *Proc., Inst. Mech. Engrs.*, London, 205, 23–28.
- Finn, W. D. L., Lee, W. K., and Martin, G. R. (1976). "An effective stress model for liquefaction." *J. Geotech. Engrg. Div.*, ASCE, 103(6), 517–533.
- Finn, W. D. L., Yogendrakumar, M., Toshida, N., and Yoshida, H. (1986). *TARA-3: A program to compute the response of 2-D embankments and soil-structure interaction systems to seismic loadings*, Dept. of Civ. Engrg., University of British Columbia, Vancouver.

- Frankel, A., and Vidale, J. (1992). "A 3-dimensional simulation of seismic waves in Santa Clara Valley, California, from a Loma Prieta aftershock." *Bull. Seismological Soc. of Am.*, 82(5), 2045–2074.
- Glaser, S. D. (1996). "Insight into liquefaction by system identification." *Géotechnique*, London, 46(4), 641–656.
- Goupillaud, P. L. (1961). "An approach to inverse filtering of near-surface layer effects from seismic records." *Geophysics*, 26(6), 754–760.
- Haag, E. (1985). "Laboratory investigation of static and dynamic properties of sandy soils subjected to the 1981 Westmoreland earthquake." *Geotech. Engrg. Rep. GR85-11*, Dept. of Civ. Engrg., University of Texas, Austin, Tex.
- Holzer, T. L., Youd, T. L., and Bennett, M. J. (1989a). "In situ measurement of pore pressure build-up during liquefaction." *Proc., 20th Joint Panel Meeting, U.S.-Japan Cooperative Program in Wind and Seismic Effects, NIST SP 760*, National Institute of Standards and Technology, Gaithersburg, Md., 118–130.
- Holzer, T. L., Youd, T. L., and Hanks, T. C. (1989b). "Dynamics of liquefaction during the 1987 Superstition Hills, California, earthquake." *Sci.*, 244, 56–59.
- Iai, S., Matsunaga, Y., and Kameoka, T. (1992). "Strain space plasticity model for cyclic mobility." *Soils and Found.*, Tokyo, 32(2), 1–15.
- Inaudi, J. A., and Kelly, J. M. (1995). "Linear hysteretic damping and the Hilbert transform." *J. Engrg. Mech.*, ASCE, 121(5), 626–632.
- Inaudi, J. A., and Makris, N. (1996). "Time-domain analysis of linear hysteretic damping." *Earthquake Engrg. and Struct. Dyn.*, 25, 529–545.
- Kanasewich, E. R. (1981). *Time sequence analysis in geophysics*, University of Alberta Press, Edmonton, Alta., Canada.
- Luco, J. E., and Apsel, R. J. (1983). "On the Green's function for a layered half-space. Part I." *Bull. Seismological Soc. of Am.*, 73, 909–929.
- Nigbor, R., and Steller, R. (1996). "Borehole geophysical measurements at GVDA." *Rep. 6597*, Agbabian Associates, Pasadena, Calif.
- Oppenheim, A. V., and Schaffer, R. W. (1989). *Discrete-time signal processing*, Prentice-Hall, Englewood Cliffs, N.J.
- Pestana, J. M., and Whittle, A. J. (1999). "Formulation of a unified constitutive model for clays and sands." *Int. J. Numer. and Analytical Methods in Geomech.*, 23, 1215–1243.
- Prevost, J. H. (1978). "Anisotropic undrained stress-strain behavior of clays." *J. Geotech. Engrg. Div.*, ASCE, 104(8), 1075–1090.
- Pyke, R. M. (1979). "Nonlinear soil models for irregular cyclic loadings." *J. Geotech. Engrg. Div.*, ASCE, 105(6), 715–726.
- Robinson, E. A., and Silvia, T. M. (1979). *Digital foundations of time series analysis, The Box-Jenkins approach*, Vol. 1, Holden-Day, San Francisco.
- Schnabel, P. B., Lysmer, J., and Seed, H. B. (1972). *SHAKE, A computer program for earthquake response analysis of horizontally layered sites, No. 72-12*, Earthquake Engineering Research Center, Berkeley, Calif.
- Seed, H. B., and Idriss, I. M. (1970). "Soil moduli and damping factors for dynamic response analyses." *EERC 70-10*, University of California, Berkeley, Calif., 1–41.
- Silvia, T. M., and Robinson, E. A. (1979). *Deconvolution of geophysical time series in the exploration for oil and natural gas*, Elsevier Science, Amsterdam.
- Streeter, V. L., Wylie, E. B., and Richart, F. E. (1973). "Soil motion computations by characteristics methods." *Proc., ASCE Nat. Struct. Engrg. Meeting*, ASCE, New York.
- Vucetic, M., and Dobry, R. (1991). "Effect of soil plasticity on cyclic response." *J. Geotech. Engrg.*, ASCE, 117(1), 89–107.
- Zeng, Y., and Anderson, J. G. (1995). "A method for direct computation of the differential seismogram with respect to the velocity change in a layered elastic solid." *Bull. Seismological Soc. of Am.*, 85(1), 300–307.

APPENDIX IV. NOTATION

The following symbols are used in this paper:

- $D_j(z)$ = DDO = $Z(e^{-ik_j h_j})$;
 dt = time step;
 E_j = upgoing wave at j th interface;
 E_{rock} = incident wave from bedrock;
 F_j = downgoing wave at j th interface;
 G_j = elastic shear modulus of j th layer;
 $\bar{G}_j(t)$ = average G of j th layer at time instant t ;
 $G_j(x_j, t)$ = G of soil element at x_j and time instant t ;
 h_j = layer thickness of j th layer;
 k_j = complex wave number of j th layer;

$T_{i-k}(z)$ = Z-domain transfer function for interface $i-k$;
 U_j = particle shear displacement at j th interface;
 U_{outcrop} = particle shear displacement at outcrop rock;
 V_j = shear-wave velocity of j th layer;
 x_j = local coordinate of j th layer;
 Z = Z transform;
 $z = e^{-i\omega dt}$;
 z^n = time delay operator of $n \cdot dt$;

α_j = impedance ratio at $(j + 1)$ th interface;
 β = damping ratio;
 γ_j = shear strain directly beneath j th interface;
 η_j = viscous damping coefficient of j th layer;
 $\bar{\eta}_j(t)$ = average η of j th layer at time instant t ;
 $\eta_j(x_j, t)$ = η of soil element at x_j and time instant t ;
 ρ_j = mass density of j th layer; and
 τ_j = shear stress directly beneath j th interface.